Available online at www.sciencedirect.com

SCIENCE DIRECT®

Remote Sensing of Environment 93 (2004) 283–295

Remote Sensing of Environment

www.elsevier.com/locate/rse

Assessing tundra–taiga boundary with multi-sensor satellite data

K.J. Ranson[a,*], G. Sun[b], V.I. Kharuk[c], K. Kovacs[d]

[a]Biospheric Sciences Branch, GSFC, NASA's Goddard Space Flight Center, Code 923, Greenbelt, MD 20771, USA
[b]Department of Geography University of Maryland, College Park, MD, USA
[c]V.N. Sukachev Institute of Forest, Academgorodok, Krasnoyarsk, Russia
[d]Science Systems and Applications, Inc., Lanham, MD, USA

Received 12 December 2003; received in revised form 18 June 2004; accepted 26 June 2004

Abstract

Monitoring the dynamics of the circumpolar boreal forest (taiga) and Arctic tundra boundary is important for understanding the causes and consequences of changes observed in these areas. This ecotone, the world's largest, stretches for over 13,400 km and marks the transition between the northern limits of forests and the southern margin of the tundra. Because of the inaccessibility and large extent of this zone, remote sensing data can play an important role for mapping the characteristics and monitoring the dynamics. Basic understanding of the capabilities of existing space borne instruments for these purposes is required. In this study we examined the use of several remote sensing techniques for characterizing the existing tundra–taiga ecotone. These include Landsat-7, MISR, MODIS and RADARSAT data. Historical cover maps, recent forest stand measurements and high-resolution IKONOS images were used for local ground truth.

It was found that a tundra–taiga transitional area can be characterized using multi-spectral Landsat ETM+ summer images, multi-angle MISR red band reflectance images, RADARSAT images with larger incidence angle, or multi-temporal and multi-spectral MODIS data. Because of different resolutions and spectral regions covered, the transition zone maps derived from different data types were not identical, but the general patterns were consistent.

Keywords: Tundra–taiga transition zone; Landsat; ETM+; MISR; MODIS; RADARSAT; Multi-spectral; Multi-angle; Temporal; Boreal forest

1. Introduction

The tundra–taiga boundary stretches for more than 13 400 km around the Northern Hemisphere and is probably the Earth's greatest vegetation transition. This transition zone is sensitive to both climate change and human activities (Callaghan et al., 2002a,b). The shifting of local subarctic tree lines throughout the forest–tundra biome, which is linked to ecological processes at different spatiotemporal scales, will reflect future global changes in climate (Payette et al., 2001). Monitoring the dynamics of this tundra–taiga boundary is critical for our understanding of the causes and consequences of the changes. The high-latitude ecosystems, i.e. boreal forests and tundra, plays an important role in the climate system (Bonan et al., 1995). Improved understanding of the role requires a concerted research efforts to be conducted over a long enough time-period to detect and quantify ecosystem feedbacks (Chapin et al., 2000). The so-called "missing sink" in the global carbon balance emphasizes a need for satellite analysis (e.g. Myneni et al., 2001), which offers much improved information on changes in the tundra–taiga transitional zone and on forest structure in this area (Rees et al., 2002).

The tundra–taiga transition area is dynamic because it is very sensitive to human activity and climate change. During the last 6000 years in northern Eurasia, there has been a general cooling trend of about 2–4 °C and Larch and birch stands retreated between 400 and 500 km southward during this period (Callaghan et al., 2002a,b). Global average

* Corresponding author. Tel.: +1 301 614 6650; fax: +1 301 614 6695.
E-mail addresses: kenneth.j.ranson@nasa.gov (K.J. Ranson), guoqing@taiga.gsfc.nasa.gov (G. Sun), kharuk@forest.akadem.ru (V.I. Kharuk), kkovacs@forest.gsfc.nasa.gov (K. Kovacs).

0034-4257/$ - see front matter © 2004 Published by Elsevier Inc.
doi:10.1016/j.rse.2004.06.019

surface air temperatures have risen by more than 0.5° since the mid 19th century (Briffa et al., 1996) and temperatures have warmed by as much as 2° in the past three decades in parts of the Northern Hemisphere (Hansen et al., 1999). If it is assumed that growth and reproduction are controlled by temperature, a rapid advance of the tree line would be predicted (Grace et al., 2002). The northward movement of tundra–taiga boundary may be the eventual outcome if climatic warming persists over centuries or millennia (Skre et al., 2002). Some studies predict that up to about one half of the tundra could be colonized by trees by 2100 (Callaghan et al., 2002a,b; Harding et al., 2001).

There is general agreement that the temperature is of major importance in determining the northern extent of the boreal forest. Widespread degradation of permafrost has been shown in numerous studies (Osterkamp & Romanovsky, 1996; Pavlov, 1994). Recent observations by Siberian and other scientists suggest that the taiga forests are expanding into the tundra, an indicator of climate warming (e.g., Kharuk et al., 1998, 2002a,b). In a case study conducted by Rees et al. (2002) in a portion of the West Siberian plain (66.5°N, 70.75°E) from 1968 to 1997, seven of their 20 test sites showed colonization by advancing forests, one showed an inconclusive shift in the treeline, and one test site, surrounded by water and wetlands, showed evidence of forest retreat. The remaining 11 sites showed no appreciable forest advance but four of these sites had developed denser forest cover. In studies of the Polar Ural mountains, Kharuk et al. (1998) found that during the period between 1968 and 1989 the crown closure of stands increased considerably (four to five times), and the tree line boundary moved 100–300 m into the tundra zone. The tree invasion into tundra areas is a slow process and is limited by low larch seed fertility (about 5–7%) and the radius of seed dispersal. Those changes were attributed to the vegetation growth period and precipitation increase. These observations are consistent with those in northern Canada, where the primary effect of climate warming has been on tree density, with only minor advance of the tree line (Payette & Gagnon, 1985). Researches have found that during the past 100–150 years, white spruce density increased in forest tundra ecotone stands in western, central and eastern Canada, but without any significant displacements of the arctic tree line (Payette et al., 2001). A study of the forest–tundra boundaries in two areas of northern Canada using Landsat imagery has also confirmed that the boreal forest extents in the areas remain basically stable (Masek, 2001).

In response to global warming, the directions of vegetation change may take place at the site level depending on local species and environmental conditions. The situation is further complicated by human activities that have led to ecosystem degradation in this area. In some case studies (Hagner & Rigina, 1998; Rees et al., 2003; Toutoubalina & Rees, 1999; Virtanen et al., 2002; Vlassova, 2002), southward displacement of the tundra–taiga boundary was reported due to human disturbance and increasing waterlogging, which led to paludification and the death of treeline trees. Local variations in climate and human activities require continued monitoring and research. The transition from taiga to tundra is characterized by a change in tree cover density and is determined by forest gradients related to the presence of the landscape such as rivers, bogs, and uplands. The tundra–taiga boundary is not a distinct edge but a transition area where patches of tundra and forest are mixed. Because the boundary is not clearly defined, it is obvious that the change of this transition zone is also difficult to quantify. Rees et al. (2002) presented several case studies for characterization and monitoring of tundra–taiga interface in Russia using Landsat and SAR data and the potential and limitations of the remote sensing technology. While optical remote sensing technology has been reasonably well established for delineation of different vegetation types, rapid phenological change is still a source of confusion when comparing images collected at different dates. Furthermore, the frequency of cloud cover at high latitudes makes the acquisition of visual and infrared images difficult. They found that at a regional scale, in order to get images within a week of the peak of the growing season each year for monitoring the transition zone, we are limited to the instruments with wide swaths such as AVHRR, Vegetation, MERIS, MODIS, MISR, WIFS, etc. Radar, due to its all-weather capability and sensitivity to forests, provides an alternative to optical technology. However, the image speckle and the sensitivity of radar image to terrain, surface roughness and moisture may cause confusion between forests and rough surfaces, especially at short wavelengths (Bourgeau-Chavez et al., 2002). Stow et al. (2004) gave an overview of multi-temporal remote sensing and the special challenges and opportunities for land cover change applications in the Arctic, and presented a series of case studies with a range of spatial resolution from 1 m to 10 km, spatial extents from 100 m to circumpolar, and time duration from months to 20 years. These studies have showed that the climatically induced changes in vegetation cover and composition in Arctic need to be monitored at different spatial scales.

Ground studies and remote sensing analysis are required to develop techniques to identify the establishment of taiga species in traditional tundra areas. In this study, we examined the capabilities of several types of remote sensing data for identifying the existing tundra–taiga transition zone. A Landsat-7 ETM+ image and IKONOS image both acquired on July 17, 2002, were used to develop a base map of the study area and other remote sensing data (SAR, MISR and MODIS) were compared to this base map.

2. Test site and data

The Ary Mas (forest island) study site is located at 72°28′ N/101°40′ E, in the tundra–taiga transition zone in

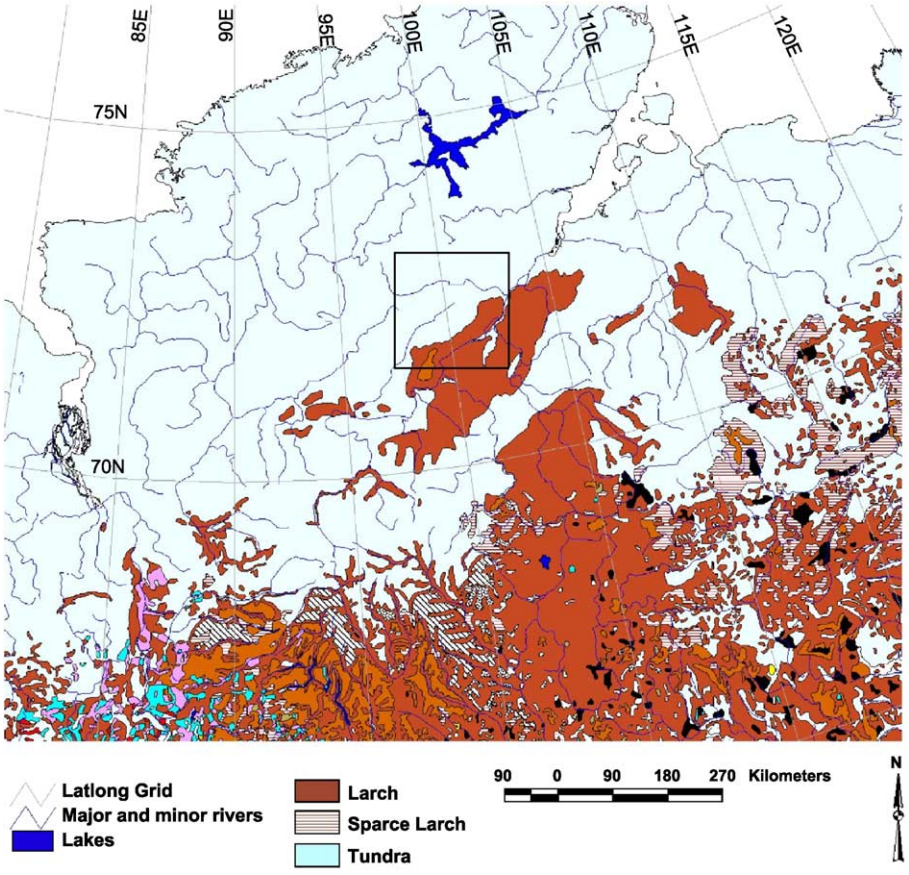

Fig. 1. 1990 forest cover map of the Ary Mas area. The square indicates the study area location.

central Siberia, Russia. Fig. 1 is a map of the area showing the study site location and general cover types from 1990 Russian forest survey information. Larch (*Larix gmelinii*) is the frontier tree species in this region. Ary Mas area is a reserve and is recognized as the farthest north known area that supports tree growth (Kharuk et al., 1998). The local elevation and hydrology affect the tree distribution, including dendritic patterns along the river valleys. There is usually not an abrupt change between forest and tundra since trees often colonize an area and slowly increase in crown cover.

Table 1 lists the satellite data used in this study. Landsat-7 ETM+ data was acquired on July 17, 2002. Fig. 2A is the Landsat-7 image with Bands 4 (0.75–0.90), 3 (0.63–0.69), and 2 (0.525–0.605) were displayed as red, green and blue, respectively. Taiga appears as red on the right side of the image and is dominated by larch and the left portion of the image is tundra. RADARSAT standard beam data at various incidence angles were acquired in August 2001 (see Table 1). Because of the higher backscattering from trees at larger incidence angles (ST5 and ST6), these forested areas appear bright in the image shown in Fig. 2B (beam ST6).

MISR (Multiangle Imaging Spectral Radiometer) is a four spectral band instrument with nine cameras positioned for fore-aft and nadir Earth viewing. MISR flies along with MODIS on the NASA EOS Terra spacecraft (Diner et al., 2002). The MISR data used in this study were acquired on July 17, 2002, a few minutes after the Landsat-7 ETM+ data

Table 1
List of remote sensing data used in the study

Data	Acquisition date	Characteristics
Landsat-7 ETM+	07-17-2002	1–7 Bands
RADARSAT ST2	08-02-2001	27.74°
RADARSAT ST3	08-05-2001	34.10°
RADARSAT ST4	08-15-2001	36.56°
RADARSAT ST5	08-08-2001	39.22°
RADARSAT ST6	08-11-2001	44.14°
IKONOS	07-17-2002	B,G,R.NIR, pan
MISR	07-17-2002	MISR reflectance in B,G,R,NIR bands, 9 look angles: DF=70.5°, CF=60.0°, BF=45.6°, AF=26.1°, AN=0°, AA=26.1°, BA=45.6°, CA=60.0°, DA=70.5°
MOD13A1	05-25-2001 to 10-16-2001	MODIS 500 m 16-day composite, NDVI, Red and MIR reflectance products

B—blue band, G—green band, R—red band, NIR—near infrared band, MIR—middle infrared.

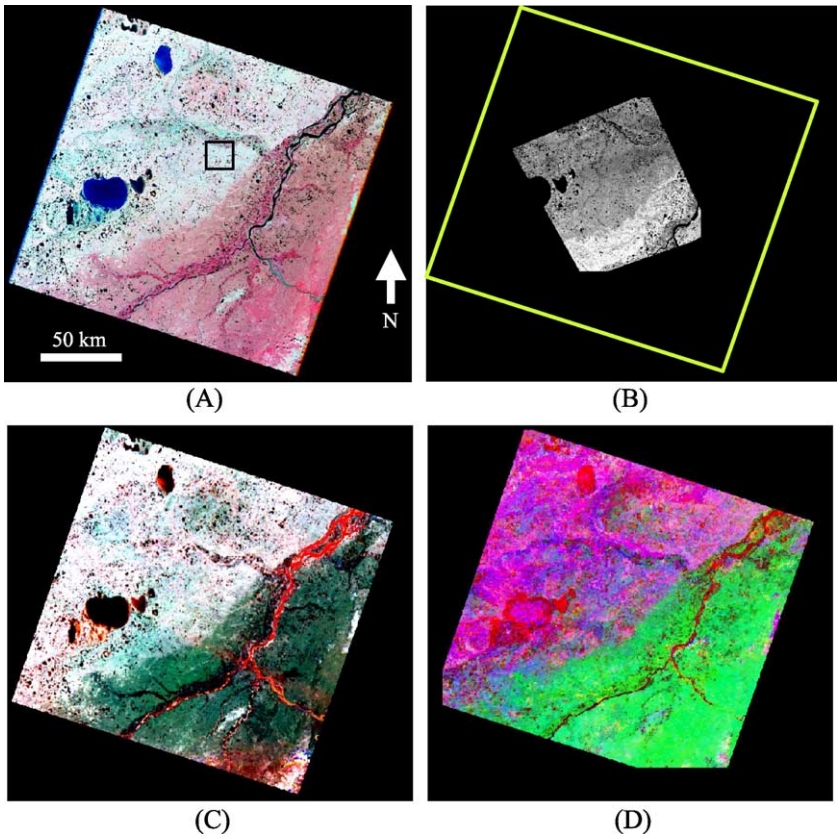

Fig. 2. Satellite images of Ary Mas study site. (A) Landsat-7 ETM+ image (07-17-2002)—Red=Band 4, Green=Band 3, blue=Band 2. (B) RADARSAT data (08/11/2001)—ST 6 (incidence angles 44°). (C) MISR Red channel image, (07/17/2002)—Red=DF camera, Green=AN camera and Blue =DA camera. (D) MODIS 500 m 16-day composite (05/25–10/16/2001): Red—spring maximum of Red band reflectance, Green—mean of NDVI, and Blue—mean of MIR band reflectance. (For interpretation of the references to colour in this figure legend, the reader is referred to the web version of this article).

were acquired. The MISR data were processed using the HDF-EOS Data Format Converter (HEG) (Raytheon System, 2003). Fig. 2C shows a false color composite image of MISR Red band data acquired at different angles. The forward-looking camera at 70.5° (DF) data is displayed as red, AN (nadir-looking) as green and DA (70.5° backward-looking) as blue. The effect of the composite of three-angle images is a clear difference between tundra and taiga in the MISR image.

The MODIS data was also from the Terra spacecraft (Guenther et al., 2002) and the multi-temporal aspects of the data were utilized. The 500 m, 16-day composite data (MOD13A1 product, Collection 4, http://modis.gsfc.nasa.gov) were acquired from the EOS Land Processes Distributed Active Archive Center. Because the 2002 MODIS data were not yet available processed to Collection 4 at the time this study was conducted, the 2001 data were used. The winter time data were affected by snow cover and low illumination so only data from early spring to fall (March to October) were used. Several statistics such as minimum, maximum, mean and standard deviation were calculated for reflectance and NDVI for the spring, summer and fall time series. Fig. 2D is a false color composite of the MODIS data with spring maximum red reflectance coded as red, NDVI summer maximum as green, and summer mean MIR reflectance as blue.

An early land cover map (Knorre, 1972) near Ary-Mas was available along with the field data from sampling plots recorded in 1969–71, 1989–91. That cover map was generated based on the ground tests plots data and of the 1:35,000 black/white aerial photography interpretation. In the year 2000 additional sampling data were acquired by Sukachev Institute of Forest personnel. However, these data cover only a small part of the area and were used for training and testing purposes. One IKONOS image acquired the same day as the Landsat7 ETM+ data within the area was also used as ground truth. Fig. 3 shows IKONOS panchromatic images of several typical targets in the area. The densest taiga in the study area was located mainly to the south of this imaged area and is not represented on the IKONOS image. The surface of the tundra is mostly covered by lichen, which has relatively high reflectance compared to the forest areas. Larch is the only tree species in this area. Because of the low Sun angle in this area, the shadows of trees are elongated and make the area significantly darker than the surroundings. The taiga area presented in Fig. 3A is relatively low density (estimated to be ~20% cover using dotgrid counting of the image) and clearly shows the

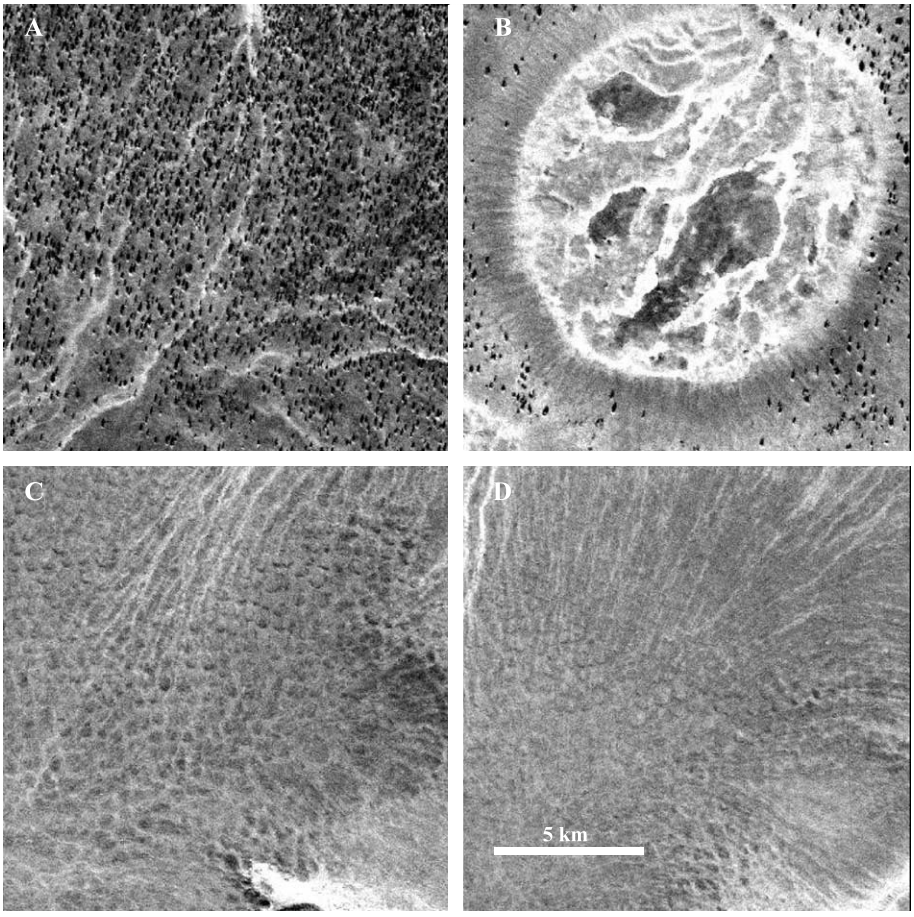

Fig. 3. IKONOS 1-m pan images of typical targets in the area. The area imaged by IKONOS is marked by the black square on ETM+ images in Fig. 2A.

shadows on the tundra background. Bogs have more complex structure and reflectance properties (Fig. 3B).

3. Data analysis methods

3.1. Georeferencing and co-registration of data

The map projection used in our study is Lambert Conformal Conic Projection (LCC, with two parallels of 50°N and 60°N, and central meridian of 90°E and WGS84 ellipsoid datum), defined for central Siberia. Landsat-7 ETM+ data was processed by ErosData Center into this LCC projection with pixel size of 30 m by cubic convolution re-sampling. The MODIS data were re-projected from Integer Sinusoidal to the LCC projection and re-sampled to a pixel size of 500 m. MISR data were received in a long strip with 180 frames. We used the software HEG developed by EOSDIS Core System Project to project it into the LCC projection and subset to our study area. Since the pixel size of MISR red band and AN cameras of other bands (blue, green and NIR) is 275 m, all MISR data were re-sampled to 275 m pixel size during the process. The geolocation errors for Landsat-7 ETM+ systematically processed data, and MODIS products are about 50 and 150 m, respectively (Wolfe et al., 2002). According to the MISR calibration results report (http://www-misr.jpl.nasa.gov/mission/geocal/migeocal.html), the RMS geolocation errors of MISR data range from 143 m (An camera) to 372 m (Da) along track, and from 115 m (An) to 185 m (Df) across track. RADARSAT (25 m pixel) data were manually registered to ETM+ data. The control points derived from river junctions and small ponds were used with a resulting error of less than two pixels.

3.2. Signatures across the tundra–taiga transition zone

The treeless tundra and taiga forest can be visually identified on almost all the channels of the data used, except the RADARSAT data at the steepest angle (ST2). A transect running north to south across the transition zone was used to show the differences in spectral information from various instruments. To zoom into the transition region and compare the changes in images of different sensors, the profiles of the most sensitive channels were registered and overlaid on the same plot as shown on Fig. 4. A vertical line on the plot identifies the center of the tundra–taiga boundary. For comparison purposes, the image value for each channel was normalized by the maximum channel value so the data would range between 0 and 1. To avoid crowding of the

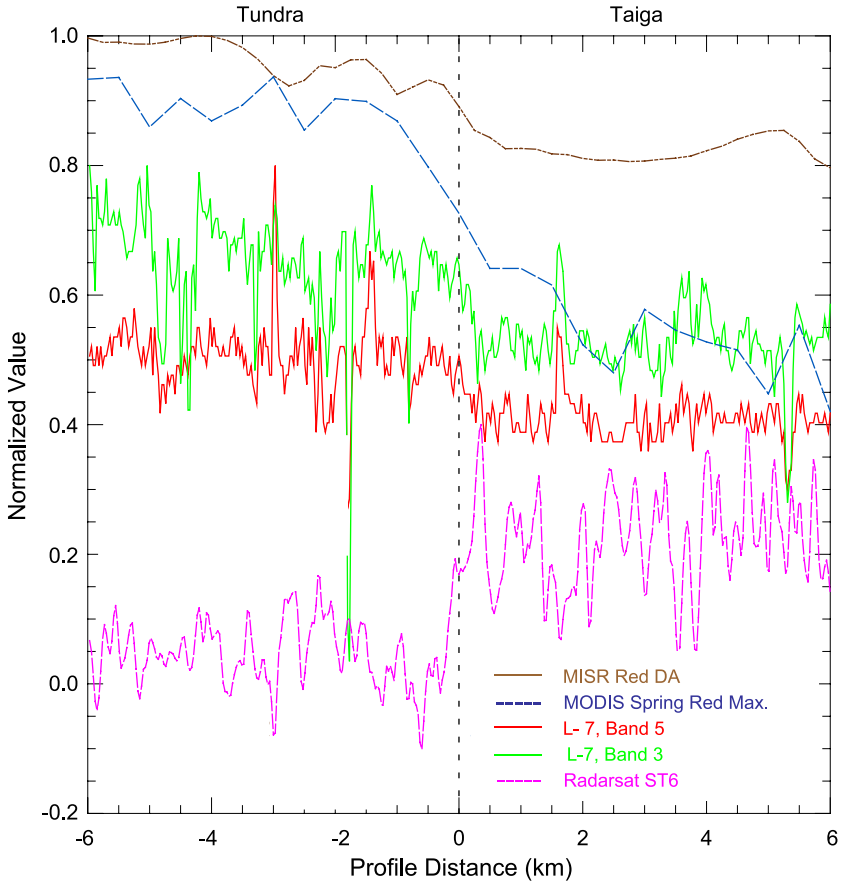

Fig. 4. Signature profiles of ETM+, RADARSAT, MISR and MODIS data across a tundra–taiga transition boundary.

plots near 1.0, the two Landsat-7 curves (bands 3 and 5) were adjusted down by 0.2, the RADARSAT curves were lowered by 0.6, and the MODIS profile was lowered by 0.1.

3.3. Tundra–taiga transition area mapping from Landsat ETM+

As we have mentioned in the introduction, the tundra–taiga transition is a gradual change from dense taiga, to taiga with patches of tundra, to tundra with patches of taiga, and finally to pure treeless tundra. The tree stem density also gradually changes across the transitional zone. Characterizing this zone requires information on tree density of the taiga stands and on the spatial patterns of the tundra–taiga mosaic structure. Because of the spatial resolution limitation of remote sensing data used in this study, spectral linear unmixing was used.

Fig. 3 illustrates that a forest stand may be considered as trees (with shadows) over the tundra background. Even for the dense stands in this area, the crown closure is relatively low. Therefore the crown shadow is always a significant factor in determining the target signature. Two end members, i.e. the dense forest stand and treeless tundra were used in the unmixing. However, areas of atypical of tundra and taiga land cover types needed to be identified and excluded from the spectral unmixing.

First, the seven-band Landsat 7 ETM+ image was classified into categories found in this area using a Maximum-Likelihood Classifier. These classes include water bodies (lakes and rivers), taiga (larch forest), tundra, bogs (shrubs and grass cover), riparian vegetation, and sand bars. IKONOS data and a land cover map were used in locating training sites. A mask image, which excluded all non-forest and non-tundra pixels, was developed from the ETM+ classification. This mask image was later used in processing of RADARSAT, MISR and MODIS data. The taiga and tundra end-members were located in the Landsat 7 ETM+ image based on the classification and image tones, and linear spectral unmixing technique was applied to all pixels of the 7-band ETM+ selected by the mask image.

Linear spectral unmixing methods have been increasingly applied in the remote sensing community to resolve the sub-pixel mixture information (Sabol et al., 2002). An important step in spectral unmixing is to identify the end-member and obtain the spectra of these end-members. Common practice is to obtain the end-member spectra manually from certain small regions in remote-sensing imagery, and then use the least-squares method to estimate the cover class proportion for each pixel (Hu et al., 1999). Researchers have found that most of the uncertainty in the unmixing results arose from the end-member creation, not

Table 2
Test results of Landsat ETM+ classification

Test area from map	Landsat ETM+ classification				Comments about classification
	Larch	Tundra	Bog	Sand bar	
Larch (higher CC)	36				Accuracy 100%, Crown closure (CC)>0.5
Larch (low CC)	63				Accuracy 100% 0.1≤CC≤0.5
Larch (very sparse)	4	32			Accuracy 11%, CC<0.1, similar to tundra
Tundra	3	42	7		Accuracy 81%
Bog	2	25	102		Accuracy 80%, confused with tundra
Sand bar				41	Accuracy 100%

from the least-square method (Sohn & McCoy, 1997). The end-member selection is the crucial step in the spectral unmixing, and some techniques such as the selection scheme by Saghri et al. (2000) have been developed to ensure the quality of end-members.

The number of the end-members should be less than (or equal to) the data channels. The limiting number of useful channels for the sensors used here was three distinct illumination angles for RADARSAT. In order to study the tundra–taiga boundary by identifying the changes of tree coverage across the transition zone, two end-members, i. e. tundra and taiga were used. All the pixels, which do not belong to tundra or taiga based on the MLC classification discussed above were excluded from analysis. The taiga end-member represents the areas with the densest trees in the study area (>0.3 crown cover). The abundance of taiga, therefore, does not necessary reflect the actual percentage of tree crown cover.

Both category types were selected from homogeneous areas, avoiding river valleys with riparian grasses and shrubs. Because the unit sum constraint was applied, the sum of the abundances of tundra and taiga should be 1.0. The abundance should be in the range of 0–1.0 in ideal situations. Actually, these values could also be negative, or

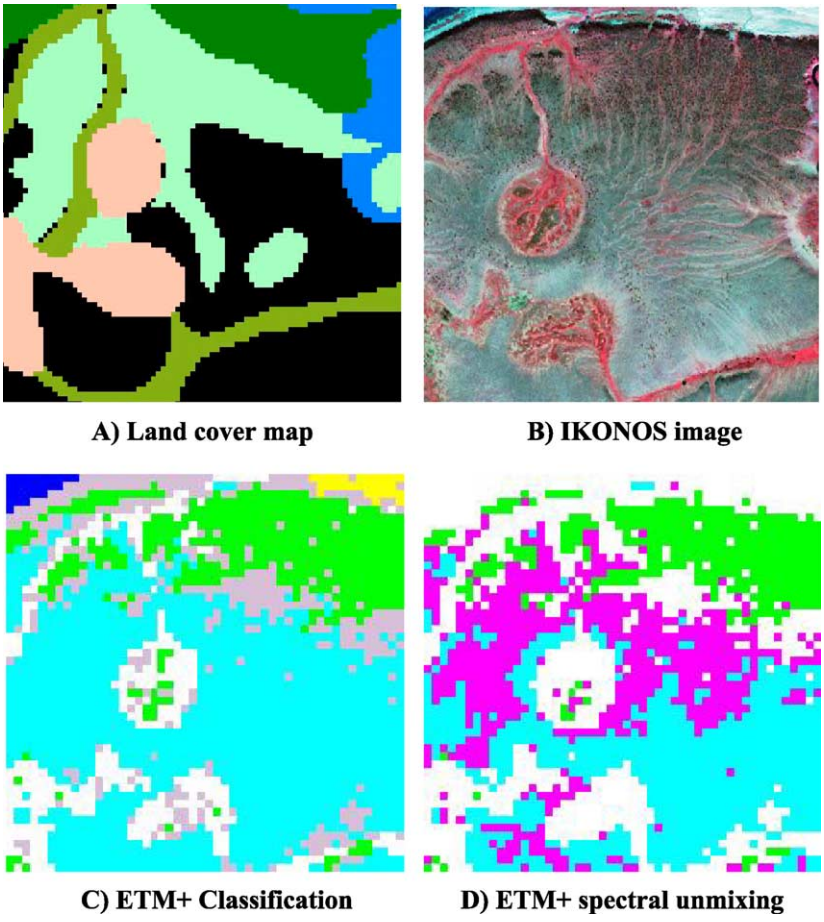

Fig. 5. Subsets of (A) Land cover map, green—taiga, light blue—grass , brown—riparian, yellow—sand bars, pink—low density larch, white—unmapped (tundra). (B) IKONOS 4 m false-color infrared image, (C) Classification of Landsat-7 ETM+ image: Green—taiga, Cyan—tundra, Dark Blue—water, White—masked out classes. (D) Color density slice of taiga abundance from linear spectral unmixing of 7-band ETM+ images with two end-members; Dark Green—Taiga abundance greater than 0.5, Magenta—Taiga abundance from 0 to 0.5, Cyan—tundra (no taiga), White—masked out. Image width represent 1.5 km on the ground. (For interpretation of the references to colour in this figure legend, the reader is referred to the web version of this article).

larger than 1.0 because of errors in the solutions of the linear equations. The linear spectral unmixing determines the relative abundance of the end. Only the abundance of taiga was used in the analysis. The linear spectral unmixing routine available from Research Systems (2002) was used for this analysis.

3.4. Mapping of the transition zone using other satellite data

3.4.1. RADARSAT data

The Radarsat standard beam data (beams 2, 3, 4, 5 and 6) were received in a complex format from the Alaska Science Facility. At the Goddard Space Flight Center, the data were converted from complex format to power, multilooked by 6×6 pixels using the ENVI software. Then, the data were converted from slant to ground range using the altitude of the platform and the near slant range distance. Finally, data were filtered using a 5×5 gamma filter, which reduces speckle while preserving edges in radar images (Shi & Fung, 1994). Since the Ary Mas area does not have a strong topographic gradient, no orthorectification was performed. The ground range SAR data then were registered to the Landsat-7 ETM+ image manually with accuracy within two pixels. Since the radar images have been co-registered with the ETM+ image, the tundra–taiga mask image, and the locations of the two end-members were directly used in linear spectral unmixing of the RADARSAT image data.

3.4.2. MISR and MODIS data

MISR (Diner et al., 2002) red band data (nine cameras) were re-sampled (using a nearest neighbor resampling) into 30 m pixels size and the overlapping area with the Landsat 7 ETM+ image was extracted. Only the red band data were used for further analysis for the following reasons: (1) the purpose of using MISR data was mainly to investigate the capability of multi-angle data for tundra–taiga zone mapping, (2) most cameras at the other bands have images with pixel size of 1.1 km instead of 275 m, and (3) the red band is useful to show the differences between taiga and tundra. The Terra MODIS science products received included a time series of Normalized Difference Vegetation Index (NDVI), Enhanced

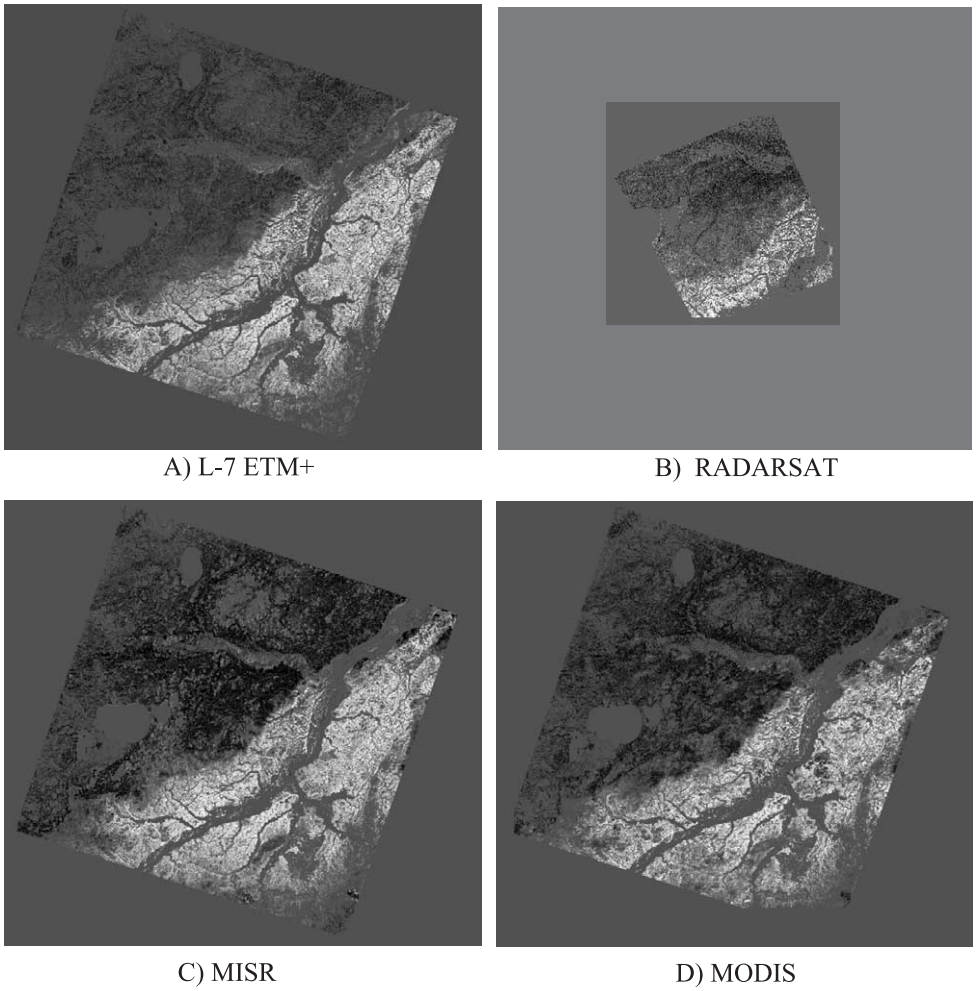

Fig. 6. Relative abundance of taiga (0–1.0, black to white) from linear spectral unmixing of (A) Landsat-7 ETM+, (B) RADARSAT, (C) MISR red band, and (D) MODIS temporal data.

Vegetation Index (EVI), and spectral reflectance of blue (channel 4), red (channel 1), near infrared (NIR, channel 2) and middle infrared, (MIR, channel 7). Only the NDVI, red and MIR data were used. For each time series, the minimum, maximum, mean and standard deviation in spring, summer and fall were calculated. By checking these channels (a total 12 for each series), six channels, which showed promise in discrimination between tundra and taiga, were selected. They were summer minimum and mean of NDVI, summer mean and spring maximum of red reflectance, summer maximum and mean of MIR reflectance. These data were also re-sampled to 30 m and the overlapping area with ETM+ data was extracted. The tundra–taiga mask image and the two end-members were used in the linear spectral unmixing of the MISR and MODIS image data.

3.5. Spatial patterns of the transition zone

To reveal the patterns of tundra–taiga composition in the transitional zone, the percentage of taiga was calculated within a moving window. The relative abundance images of taiga generated by linear spectral unmixing (Fig. 6) have a 30-m pixel size. The original data has different pixel sizes (i.e., 25 m for RADARSAT SAR data, 30 m for ETM+, 275 m for MISR and 500 m for MODIS data), these results were difficult to compare directly. We used a moving window of 33×33 pixels, and calculated the abundance of taiga within the window. If the center pixel was masked out during the process, the new pixel value was set to the value representing the background. The linear spectral unmixing process produced about 0.5% pixels with negative values for the abundance of the taiga. These values were set to zero (tundra) when calculating the average abundance in the moving window. Therefore the average abundance will be the sum of all positive values in the window and divided by the number of pixels that were not masked out during the linear spectral unmixing. The resulting images still have a pixel size of 30 m, but represent the information in a 1 km (990 m) window. These results will be more comparable since the information they show is at a similar spatial scale. The abundances of taiga were also calculated for the various window sizes within a transect placed across the boundary.

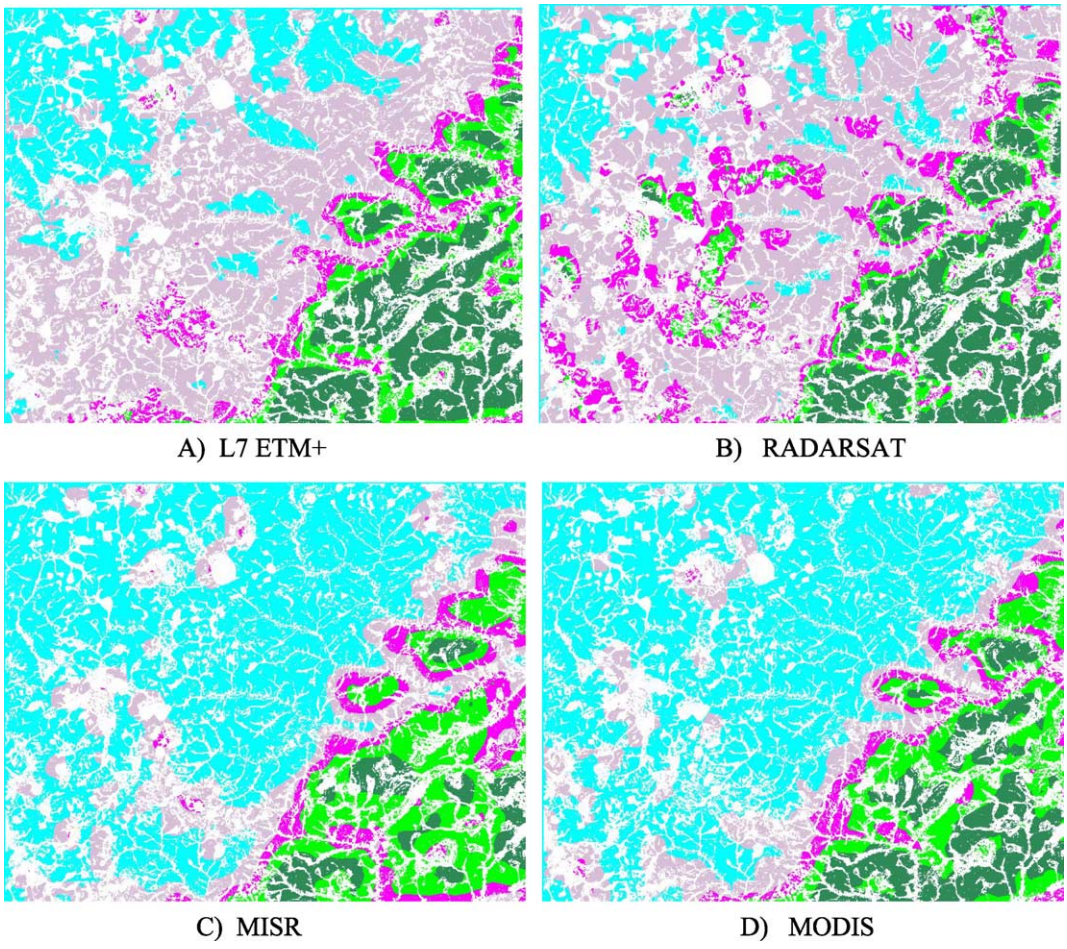

Fig. 7. Comparisons of mapped current tundra–taiga transition zone from (A) Landsat-7 ETM+, (B) RADARSAT multi-beam data, (C) MISR red band, and (D) MODIS temporal NDVI, red and MIR reflectance. Taiga abundance was calculated using a 1-km moving window and color density sliced: cyan—<0.0, gray—0–0.25, Magenta—0.25–0.5, light green—0.5–0.75, and dark green—>0.75. (For interpretation of the references to colour in this figure legend, the reader is referred to the web version of this article).

4. Results

4.1. Spectral signatures across the tundra–taiga boundary

The spectral response from the tundra–taiga ecotone was found to vary with surface and satellite type. The spectral composite images shown in Fig. 2 highlight some of these differences. Landsat7 ETM+ false-color band 4, 3, 2 combination shows increasing vegetation response from tundra to taiga (diagonally up-left to bottom-right in Fig. 2A). Radar backscattering is mostly controlled by plant water content and the surface roughness, therefore the lack of trees makes the tundra appear smoother and thus darker than the taiga (Fig. 2B). At a steeper incidence angle (ST2), backscattering from all surfaces is relatively high. When the incidence angle increases as (i.e. ST5 and ST6) the backscattering from smoother surfaces, i.e. tundra, decreases. The multi-angle red band image from MISR also shows differences across the transition zone. Here the tundra is relatively bright in all bands, but the forest areas appear darker because of absorption by the larch needles and shadows cast by the trees. Because of Terra's descending orbit and because the solar illumination was coming from the south (~40° elevation, ~180° azimuth), the DF camera received high reflectance from glint from the water surface (seen as red lakes in Fig. 2C), while the DA camera was near the hot-spot position. The MODIS data clearly shows the taiga areas against the tundra (lower NDVI and higher red and MIR reflectance).

The profiles of normalized signatures for a set of selected channels in Fig. 4 show the capabilities of each sensor for discriminating between forest and non-forest areas. For example, the red and middle-infrared bands of Landsat-7 ETM+ show obvious transition from tundra to taiga. The MISR red band data (especially the AN and the afterward cameras) show a difference between tundra and taiga. Statistical parameters (such as minimum and maximum, mean and standard deviation) of the temporal MODIS data were also found to be useful for tundra–taiga transition zone mapping. The RADARSAT ST6 data shows that the backscattering is lower for smoother tundra surface and higher for the taiga. The ST6 data also shows a great deal of change across the boundary region. In addition to vegetation change, other factors such as elevation, ground surface roughness and hydrological conditions may also play a role here. For the MISR red band, signatures from both forward (DF, not shown) and backward (DA, shown in Fig. 4) cameras exhibited more change than the nadir looking image (not shown). Among the nadir looking MISR (275 m resolution) images, the red band shows the most significant change, consistent with Landsat-7 ETM+ data. The change patterns of ETM+ band 3 (red curve) and MISR red band DA image (black curve) are similar. The MODIS maximum red-band reflectance during spring time shows higher values for tundra areas with a sharp decrease across the boundary into the taiga. All the sensor channels shown in Fig. 4 recorded a change across the transition zone.

Table 3
Results of MODIS taiga abundance classification relative to Landsat

MODIS classified as	Landsat class				
	Tundra	0–0.25	0.25–0.5	0.5–0.75	Taiga
Tundra	96.5	82.1	21.4	1.1	0.0
0–0.25	3.47	17.2	35.1	5.1	0.5
0.25–0.5	0.0	0.7	35.7	26.1	2.1
0.5–0.75	0.0	0.0	7.7	54.8	37.0
Taiga	0.0	0.0	0.1	12.9	60.4
Unclassified	0.0	0.0	0.0	0.0	0.0

Table 4
Results of MISR taiga abundance classification relative to Landsat

MISR classified as	Landsat Class				
	Tundra	0–0.25	0.25–0.5	0.5–0.75	Taiga
Tundra	96.6	81.9	9.5	0.0	0.0
0–0.25	3.4	17.5	52.7	8.1	0.0
0.25–0.5	0.0	0.6	35.6	44.3	7.0
0.5–0.75	0.0	0.0	2.3	45.8	62.5
Taiga	0.0	0.0	0.0	1.8	30.5
Unclassified	0.0	0.0	0.0	0.0	0.0

4.2. Tundra–taiga transition zone mapping from remote sensing data

4.2.1. Landsat-7 classification

The Landsat-7 ETM+ image was classified using a MLC with the training sites selected based on a land cover map, the IKONOS image, and the visual interpretation of ETM+ false color images. The classification accuracy for the training sets was high. In fact, by using a water mask, the MLC classification using six categories (taiga, tundra, bog, grassland, riparian vegetation, and sand-bar) approached 100% for the training sites. For additional testing, pixel arrays for map categories were selected from a land cover map and these mapped classes compared with the Landsat 7 MLC classification. Taiga and tundra areas showed high classification accuracy (Table 2). The very sparse larch stands were greatly confused as tundra (only 11% correct classification), and bog areas were sometimes confused with tundra (~20% of the time). These comparisons and the subset images in Fig. 5 show that the tundra and taiga areas have been separated from the other classes. These results

Table 5
Results of RADARSAT taiga abundance classification relative to Landsat results

Radarsat classified as	Landsat class				
	Tundra	0–0.25	0.25–0.5	0.5–0.75	Taiga
Tundra	42.7	7.8	1.2	0.0	0.0
0–0.25	53.0	67.6	39.8	0.9	0.0
0.25–0.5	0.6	21.1	44.7	23.5	0.5
0.5–0.75	0.0	3.1	13.1	37.1	6.2
Taiga	0.0	0.4	1.2	38.4	93.32
Unclassified	3.7	0.0	0.0	0.0	0.0

also indicate that a reasonable mask was generated from the classification that isolated areas of tundra and taiga. The classification results are consistent with those discussed by Rees et al. (2002) for a taiga tundra area farther to the west (64–66°N, 75°E) in Siberia.

The comparisons of land cover map, IKONOS image, classification and linear spectral unmixing results from ETM+ were illustrated in Fig. 5. We applied level slicing to the taiga abundance image to define three classes: (1) *tundra*—the abundance of taiga is less or equal to zero (blue), (2) *taiga*—the abundance of taiga is greater than 0.3 (dark green), and (3) *transition*—the abundance of taiga is between 0.0 and 0.3 (magenta). Both the classification and spectral linear unmixing from ETM+ data show consistent

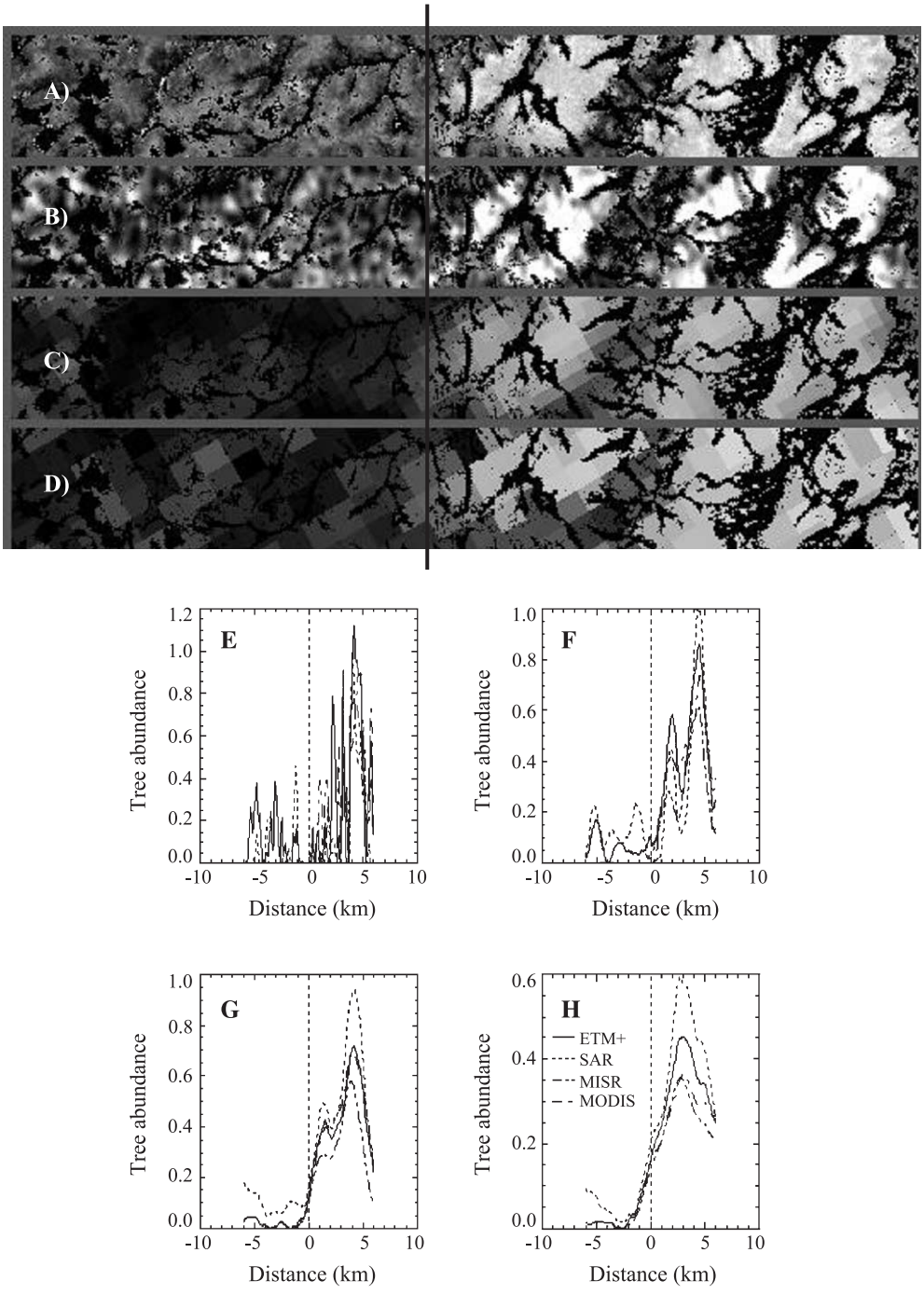

Fig. 8. Images A–D show taiga abundances calculated for a transect crossing the tundra–taiga transition from ETM+, RADASAT, MISR and MODIS data, respectively. Taiga abundances are plotted for each data type using various window sizes: (E) using a 90 m moving window, (F) 510 m window, (G) 990 m window, and (H) 2010 m window. The vertical lines in images (A–D) correspond to the dashed vertical line in graphs.

pattern of the tundra–taiga distribution vis a vis the IKONOS images in Fig. 5.

4.2.2. Linear spectral unmixing

The linear spectral unmixing determines the relative abundance of the end-member within a pixel. The linear spectral unmixing results for ETM+ are shown in Fig. 6A. In this case the results are shown as grey levels of taiga abundance from 0.0 (black) to 1.0 (white). The RADARSAT ST4-6 data, the MISR Red band data for all nine cameras, and the six MODIS time series data indices were also linearly unmixed to calculate the abundance of taiga forest. These images were re-sampled to 30 m, and the Landsat-7 mask was used to process the same pixels in the overlapped area. These results are shown in Fig. 6. The results from the MISR and the MODIS data closely resemble the results from the Landsat-7 ETM+ data. Even though the gamma filter has been used to smooth the radar data, the results show more variance, and may include terrain and surface roughness effects.

The taiga abundance were calculated using a 1-km moving window and the resulting image was color density sliced into five classes as shown in Fig. 7. The results from both MISR and MODIS data have a similar pattern for the transition zone. This is shown with magenta and gray colorings in Fig. 7.

A comparison of classification results for MODIS, MISR and RADARSAT and Landsat-7 is shown in Table 3–5. The classes used were the density-sliced categories in Fig. 7. The L-7 ETM+ results were used as "true" classes. The tundra was accurately identified by MODIS (96.5%) and MISR (96.6%), but not by the SAR (42.7%). This indicates that the treeless tundra area was quite homogeneous in terms of surface reflectance, so the sensor's spatial resolution doesn't matter much. But due to the possible heterogeneity of the surface roughness and moisture contents, and the SAR speckle, many tundra pixels appeared to have some trees, so more than half (53%) of the tundra pixels went to the class with 0–25% taiga. On the other hand, SAR identified most of the taiga pixels (93.3%), but MODIS and MISR did poorly (60.4% and 30.5%, respectively). The rest of the taiga pixels were assigned to the category with taiga abundance of 0.5–0.75. This indicates that at the 1-km scale, the taiga was not very dense and homogeneous, but had patches of tundra or other types of gaps. The accuracy of other classes between tundra and taiga varies. But mostly, they were confused with the neighboring classes, likely because the class definition between them were arbitrarily selected.

The abundance profiles were also calculated across the boundary using various window sizes. Fig. 8 shows four of these profiles using window sizes of 90, 510, 990 and 2010 m, respectively. When the window is small (90 m), both Landsat and SAR show the details of the change, which were not shown in the low-resolution MISR and MODIS data. When the window size is above 500 m, the transition patterns from Landsat, MISR and MODIS were similar.

5. Conclusions

This study has shown that data from Landsat7 ETM+, MISR red band multi-angle data, MODIS time series data, and RADARSAT large-incidence angle images are all sensitive to the surface and vegetation structure change in tundra–taiga transition zone in our study area. The location of the transition zone from images with very different spatial resolutions was consistent. The implication is that global coverage available from RADARSAT may be used for analysis where high resolution is required and cloud cover or low illumination precludes the use of Landsat-like data. Current Landsat-7 coverage problems caused by the scan line corrector malfunction make this option especially useful. For MISR the utility may be limited by frequent cloud cover and the infrequent coverage of MISR. The results suggest that MODIS may be an appropriate tool for wide area mapping of the ecotone and if the longer term record persists, monitoring of the ecotone. To increase accuracy, Landsat data or other high or moderate resolution data is needed for training purposes. The 500 m data sets used in this study provided useful information, but more work is needed. Further studies will reveal the effectiveness of 250 m two channel MODIS data sets. Our future studies will include mapping and characterization of other parts of this transition zone from these remotely sensed data.

Acknowledgments

This work funded in part by NASA Earth Science Enterprise and Russian Fund of Fundamental Investigations. The IKONOS data were acquired by Space Imaging and procured as part of the NASA Scientific Data Buy.

References

Bonan, G. B., Chapin, F. S., & Thompson, S. L. (1995). Boreal forest and tundra ecosystems as components of the climate system. *Climate Change*, *29*(2), 145–167.

Bourgeau-Chavez, L. L., Kasischke, E. S., Brunzell, S., Mudd, J. P., & Tukman, M. (2002). Mapping fire scars in global boreal forests using imaging radar data. *International Journal of Remote Sensing*, *23*(20), 4211–4234.

Briffa, K. R., Jones, P. D., Schweingruber, F. H., Karlen, W., & Shiyatov, S. G. (1996). Tree-ring variables as a proxy-climate indicators: Problems with low-frequency signals. In P. D. Jones, R. S. Bradley, & J. Jouzal (Eds.), *Climate variations and forcing mechanisms of the last 2000 years*. *NATO ASI Series: I. Global Environmental Change*, *vol. 41*, New York: Springer. 649 pp.

Callaghan, T. V., Crawford, R. M. M., Eronen, M., Hofgaard, A., Payette, S., Rees, W. G., Skre, O., Sveinbjornsson, J., Vlassova, T. K., & Werkman, B. R. (2002a). The dynamics of the tundra–taiga boundary: An overview

and suggested coordinated and integrated approach to research. *AMBIO Special Report*, *vol. 12* (pp. 3–5). Stockholm: Tundra–Taiga Treeline Research.

Callaghan, T. V., Werkman, B. R., & Crawford, R. M. M. (2002b). The tundra–taiga interface and its dynamics: Concepts and applications. *AMBIO Special Report*, *vol. 12* (pp. 6–14). Stockholm: Tundra–Taiga Treeline Research.

Chapin, F. S., McGuire, A. D., Randerson, J., Pielke, R., Baldocchi, D., Hobbie, S. E., Roulet, N., Eugster, W., Kasischke, E., Rastetter, E. B., Zimov, S. A., & Running, S. W. (2000). Arctic and boreal ecosystems of western North America as components of the climate system. *Global Change Biology*, *6*, 211–223.

Diner, D. J., Beckert, J. C., Bothwell, G. W., & Rodriguez, J. I. (2002, July). Performance of the MISR instrument during its first 20 months in Earth orbit. *IEEE Transactions on Geoscience and Remote Sensing*, *40*(7), 1449–1466.

Grace, J., Berninger, F., & Nagy, L. (2002). Impacts of climate change on the tree line. *Annals of Botany*, *90*(4), 537–544.

Guenther, B., Xiong, X., Salomonson, V. V., Barnes, W. L., & Young, J. (2002, Nov 16–30). On-orbit performance of the Earth Observing System Moderate Resolution Imaging Spectroradiometer; first year of data. *Remote Sensing of Environment*, *83*(1-2).

Hagner, O., & Rigina, O. (1998). *Detection of forest decline in Monchegorsk area*. *Remote Sensing of Environment*, *63*(1), 11–23.

Hansen, J., Ruedy, R., Glascoe, J., & Sato, Mki. (1999). GISS analysis of surface temperature change. *Journal of Geophysical Research*, *104*, 30997–31022.

Harding, R., Kuhry, P., Christensen, T. R., Sykes, M. T., & Dankers, R. (2001). Climate feedbacks at the taiga/tundra interface. *AMBIO Special Report*, *vol. 12* (pp. 47–55).

Hu, Y. H., Lee, H. B., & Scarpace, F. L. (1999). Optimal linear spectral unmixing. *IEEE Transactions on Geoscience and Remote Sensing*, *37*(1), 639–644.

Kharuk, V. I., Ranson, K. J., Tret'yakova, V., & Shashkin, E. A. (2002a). Reaction of the larch dominated communities on climate trends. In L. E. Paques (Ed.), *Proceedings of an International Symposium* "*Improvement of Larch (Larix sp.) for better growth, stem form and wood quality*". *France Gap, September 16–21* (pp. 289–295). INRA.

Kharuk, V. I., Shiyatov, S. G., Kasishke, E., Fedotova, E. V., & Naurzbaev, M. M. (2002b). Forest–tundra ecotone response to climate change. In Y. A. Izrael, et al. (Eds.) *Problems of ecological monitoring and ecosystem modeling*, *vol. XVIII* (pp. 234–260). St. Petersburg, Gidrometeoizdat: Institute of Global Climate and Ecology of Federal Service of Russia for Hydrometeorology and Environmental Monitoring and Russian Academy of Sciences.

Kharuk, V. I., Shiyatov, S. G., Naurzbaev, M. M., & Fedotova, E. V. (1998, Sept 21–23). Forest–tundra ecotone response to climate change. In Severin Woxhott (Ed.), *Proceeding of IBFRA-98* (pp. 19–23). Oslo, Norway: Oslo.

Knorre, A. V. (1972). The generalized sketch-map of the Ary-Mas larch forest. *Report on the geobotany, forests, climate and dendrochronology investigations in the Ary-Mas area*. Leningrad, Russia: The Central Committee on the Reserves at Russian Federation Government and the Botany Institute of Russian Academy of Sciences, 99 pp.

Masek, J. G. (2001). Stability of boreal forest stands during recent climate change: evidence from Landsat satellite imagery. *Journal of Biogeography*, *28*(8), 967–976.

Myneni, R. B., Dong, J., Tucker, C. J., Kaufmann, R. K., Kauppi, P. E., Liski, J., Zhou, L., Alexeyev, V., & Hughes, M. K. (2001). A large carbon sink in the woody biomass of northern forests. *Proceedings of the National Academy of Sciences of the United States of America*, *98*(26), 14784–14789.

Osterkamp, T. E., & Romanovsky, V. E. (1996). Impacts of thawing permafrost as a result of climatic warming. *EOS, Transactions, AGU*, *77*(46), F188.

Pavlov, A. V. (1994). Current changes of climate and permafrost in the Arctic and Sub-Arctic of Russia. *Permafrost and Periglacial Processes*, *5*, 101–110.

Payette, S., Fortin, M., & Gamache, I. (2001). The subarctic forest–tundra: the structure of a biome in a changing climate. *Bioscience*, *51*(9), 709–718.

Payette, S., & Gagnon, R. (1985). Late Holocene deforestation and tree regeneration in the forest–tundra of Quebec. *Nature*, *313*, 570–572.

Raytheon Systems Company. (2003). HDF-EOS Data Format Converter (HEG) Users Guide, v 1.0, Technical Paper 170-TP-013-001, January, 2003.

Rees, G., Brown, I., Mikkola, K., Virtanen, T., & Werkman, B. (2002). How can the dynamics of the tundra–taiga boundary be remotely monitored? *AMBIO Special Report*, *vol. 12* (pp. 56–62). Stockholm: Tundra–Taiga Treeline Research.

Rees, W. G., Williams, M., & Vitebsky, P. (2003, Jun 15). Mapping land cover change in a reindeer herding area of the Russian Arctic using Landsat TM and ETM+imagery and indigenous knowledge. *Remote Sensing of Environment*, *85*(4), 441–452.

Research Systems Inc. (2000). ENVI User's Guide, Version 3.4. Boulder, CO, 930 pp.

Sabol, D. E., Gillespie, A. R., Adams, J. B., Smith, M. O., & Tucker, C. J. (2002). Structural stage in Pacific Northwest forests estimated using simple mixing models of multispectral images. *Remote Sensing of Environment*, *80*(1), 1–16.

Saghri, J. A., Tescher, A. G., Jaradi, F., & Omran, M. (2000). A viable end-member selection scheme for spectral unmixing of multispectral satellite imagery data. *Journal of Imaging Science and Technology*, *44*(3), 196–203.

Shi, Z., & Fung, K. B. (1994). A comparison of digital speckle filters. *Proceedings of IGARSS'94, August 8–12* (pp. 2129–2133). Houston, Texas: IEEE International Geoscience and Remote Sensing Society.

Sohn, Y. S., & McCoy, R. M. (1997). Mapping desert shrub rangeland using spectral unmixing and modeling spectral mixture with TM data. *Photogrammetric Engineering and Remote Sensing*, *63*(6), 707–716.

Skre, O., Baxter, R., Crawford, R. M. M., Callaghan, T. V., & Fedorkov, A. (2002). How will the tundra–taiga interface respond to climate change? *AMBIO Special Report*, *vol. 12* (pp. 37–46). Stockholm: Tundra–Taiga Treeline Research.

Stow, D. A., Hope, A., McGuire, D., Verbyla, D., Gamon, J., Huemmrich, F., Houston, S., Racine, C., Sturm, M., Tape, K., Hinzman, L., Yoshikawa, K., Tweedie, C., Noyle, B., Silapaswan, C., Douglas, D., Griffith, B., Jia, G., Epstein, H., Walker, D., Daeschner, S., Patersen, A., Zhou, L., & Myneni, R. (2004, Feb 15). Remote sensing of vegetation and land-cover change in Arctic tundra ecosystems. *Remote Sensing of Environment*, *89*(3), 281–308.

Sturm, M., Racine, C., & Tape, K. (2001). Climate change-increasing shrub abundance in the Arctic. *Nature*, *411*, 445–459.

Toutoubalina, O. V., & Rees, W. G. (1999). Remote sensing of industrial impact on Arctic vegetation around Noril'sk, northern Siberia: Preliminary results. *International Journal of Remote Sensing*, *20*(15–16), 2979–2990.

Virtanen, E., Mikkola, K., Patova, E., & Nikula, A. (2002). Satellite image analysis of human caused changes in the tundra vegetation around the city of Vorkuta, north-European Russia. *Environmental Pollution*, *120*, 647–658.

Vlassova, T. K. (2002). Human impacts on the tundra–taiga zone dynamics: the case of the Russian lesotundra. *AMBIO Special Report*, *vol. 12* (pp. 30–36). Stockholm: Tundra–Taiga Treeline Research.

Wolfe, R. E., Nishihama, M., Fleig, A. J., Kuyper, J. A., Roy, D., Storey, J. C., et al. (2002). Achieving sub-pixel geolocation accuracy in support of MODIS land science. *Remote Sensing of Environment*, *83*, 31–49.